Acta Cryst. (1998). A**54**, 859–872

Crystal Growth and Crystallography

A. A. Chernov

Universities Space Research Association (USRA), 4950 Corporate Drive, Suite 100, Huntsville, AL 35805, USA, and Institute of Crystallography, Russian Academy of Sciences, 117333 Moscow, Russia.
E-mail: alex.chernov@msfc.nasa.gov

(*Received 23 April 1998; accepted 22 June 1998*)

Abstract

Selected topics that may be of interest for both crystal-structure and crystal-growth communities are overviewed. The growth of protein crystals, along with that of some other compounds, is one of the topics, and recent insights into related phenomena are considered as examples of applications of general principles. The relationship between crystal growth shape and structure is reviewed and an attempt to introduce semiquantitative characterization of binding for proteins is made. The concept of kinks for complex structures is briefly discussed. Even at sufficiently low supersaturations, the fluctuation of steps may not be sufficient to implement the Gibbs–Thomson law if the kink density is low enough. Subsurface ordering of liquids and growth of rough interfaces from melts is discussed. Crystals growing in microgravity from solution should be more perfect if they preferentially trap stress-inducing impurities, thus creating an impurity-depleted zone around themselves. Evidently, such a zone is developed only around the crystals growing in the absence of convection. Under terrestrial conditions, the self-purified depleted zone is destroyed by convection, the crystal traps more impurity and grows stressed. The stress relief causes mosaicity. In systems containing stress-inducing but poorly trapped impurities, the crystals grown in the absence of convection should be worse than those of their terrestrial counterparts.

Professor Dr A. A. Chernov has been a member of the Russian Academy of Sciences (RAS) since 1987. His scientific interests are materials and surface sciences, and crystal growth. He is Head of the Division of Elementary Processes of Crystal Growth and Real Crystal Structure at the Institute for Crystallography of RAS and Vice-President of the International Organization for Crystal Growth (IOCG). At present, he is Director of the Alliance for Microgravity Material Science and Applications at USRA and NASA Marshall Flight Center. He is an Associate Editor of the Journal of Crystal Growth and Crystal Research Technology. He has won the F. C. Frank Prize of the IOCG, Prize of the Russian Government, the E. S. Fyodorov Prize of RAS and the A. V. Shubnikov Prize of the ICRAS.

1. Introduction

'There is no crystallography without crystals' – this was the basic principle of Academician A. V. Shubnikov when he was building The Institute of Crystallography in the 1920s through 1950s in St Petersburg and later in Moscow. On the other hand, there is no way to grow crystals without crystallography, physics and chemistry. Therefore, the triad crystal growth, crystal structure and crystal properties is the real basis of modern crystallography as is reflected in the structure of the International Union of Crystallography.

It is relatively easy to grow low-quality mm–cm size inorganic and simple organic crystals. However, it took years to grow a meter long 30 cm in diameter dislocation-free pure silicon crystal from the melt for electronics, or 50 cm edge-length KH_2PO_4 (KDP) crystals from solution to multiply the frequency of powerful laser radiation, or tens of cm long man-made quartz and mica crystals. We still use natural calcite for optical devices. Nobody has grown really perfect high-T_c superconductor crystals. Growing nm-scale semiconductor and magnetic films, quantum wells, wires and dots did and does involve billions of dollars of effort and still has a long way to go. It took years to grow the first blue laser-emitting diode even with the knowledge of how to grow the red one. Again, not much science is needed to grow mediocre crystals but high technology demands high science.

Biology, the science of the 21st century, demands perfect crystals built of countless biological macromolecules. Understanding and control of crystallization of slightly soluble biominerals, like calcium phosphates, carbonates, urates, citrates *etc.* remain the problem addressed mainly at the qualitative or semiquantitative level. These salts of numerous crystallographic modifications form human bones, teeth, kidney and gall stones, mollusc shells *etc.*

The obvious importance of crystallography for crystal growth is to provide a structural background to address growth phenomena on a molecular level. The Bravais–

Donnay–Harker law, which allows one to imagine the crystal habit from crystal structure, is the classical example. These laws are only qualitatively understood as well as the periodic bond chain (PBC) and related connected net approaches (§§2.1, 2.2). However, a quantitative application of these approaches to complex structures, inorganic and protein, the influence of crystallization chemistry and temperature leave us with problems. In the last few decades, diffraction at a surface together with atomic force microscopy brought us closer to the point where the molecules, ions and atoms adjust to a crystal lattice on the way from mother liquid or gas (§§2.3, 2.4, 2.5). What is still missing here is energetics and a major part of kinetics on a molecular level.

Diffraction from liquids, unfortunately, has not yet provided a real spatial and temporal picture of the behavior of liquids, especially with respect to crystallization. However, we are now pretty sure that smectic-like liquid ordering near a crystal surface exists (§2.5) and makes it possible to guess what its kinetic consequences are if we make use not only of static but also of dynamic structure factors (§§3, 4). In this case, however, there is still a problem to ascribe each atom, at each moment, to either a liquid or a crystal phase.

Another area where diffraction crystallography and crystal growth are traditional mutual beneficiaries is crystal characterization (§5), revealing (both *in situ* and *ex situ*) dislocations and mosaicity, stacking faults, sectorial and striational inhomogeneities induced by point defects appear during the growth processes. It is not possible to reveal the microscopic nature of stress centers (§5.2) inducing internal stress and mosaicity of biocrystals by diffraction techniques. However, a crystal structure solved to a high resolution in combination with biochemical purification methods might be useful to understand the crystal growth processes preventing high crystal quality (§5.2). In solving this problem, crystallography of possible molecular conformations, that of intermolecular binding, including binding with relevant impurities, will be useful for crystal-growth science and protocols. Twinning, especially in II–VI semiconductors, is one of the thus far insufficiently addressed problems of crystal growth where *in situ* diffraction studies, like earlier work on *in situ* X-ray topography, may result in understanding the essence of twinning on the microscopic and not only on the phenomenological level. Of course, the problems discussed in this overview reflect only the author's preferences and opinions and do not cover numerous interesting subjects and achievements.

2. Faceted growth

2.1. *Crystal habit – background and challenges*

The correspondence between crystal structure and growth shape is probably the major application of structural crystallography and structural crystal chemistry to faceted crystal growth. First came the Bravais idea that the crystal habit should include the crystallographically simplest faces within which the surface density is the highest. Donnay and Harker noted that for calculation of the actual atomic densities in the planes the conventional interplanar spacings are not sufficient. One should take into account the screw symmetry axes and glide reflection planes parallel to the faces under consideration. *E.g.*, if a screw axis of the *n*th order is normal to a face, the actual particular density is n times lower than that corresponding to the full lattice period along this axis. In other words, for, say, a (0001) face of quartz, the density of SiO_2 molecules in each actual lattice layer is $n = 3$ times lower. Correspondingly, the growth rate is expected to be 3 times higher. Therefore, the basal (0001) face does not show up in the growth shape, as one might predict just from lattice spacing. This text-book example demonstrates the success of the geometrical approach to predict crystal habit.

Introduction of the periodic bond chain (PBC) concept (Hartman, 1973) provided a very efficient tool to analyze and predict crystal habit by introducing bond strengths rather that only atomic densities in crystal planes. Later, the PBC concept naturally developed into the connected net consideration (Bennema, 1993).

The simple physical basis of the PBC approach is as follows. A face grows only by generation and propagation of steps because only the steps contain the kink position in which a building unit possesses exactly half of the bonds with crystal neighbors, as compared to the same unit in the crystal bulk. Thus, this is the unit in the kink that has the chemical potential of the crystal, or, put differently, the addition of a new unit to the kink does not change the surface energy. The steps are generated either by two-dimensional (2D) nucleation or by screw dislocations. This is the most difficult and thus essentially rate-determining process. The step-generation rates in both of these modes are lower the higher the free energy of the steps. The faces on which the step generation rate is lower grow more slowly relative to the others. For clear geometrical reasons, the slowest growing faces are typically the largest on a crystal. For these faces, the unit-cell-thick slice parallel to the face includes the strongest periodic bond chains. Therefore, these faces bear the most energy-rich steps because creation of steps on these faces is associated with breaking the strongest bonds. However, the face rate depends not only on the step generation but also on the step propagation rate. This issue is still ambiguous. The velocity at which the step propagates along the face is associated with the usually unknown activation energy and entropy barriers involved in the attachment of new species to the lattice at the kink sites and the rate of the kink generations themselves. The latter is the lowest for the step orientations parallel to the strongest bond chains along the face. However, the kink density may be high enough because the barrier for kink nucleation is

Table 1. *Bonds and their energies across and within various crystallographic planes of orthorhombic lysozyme crystal (Oki et al., 1998)*

Actual magnitudes of V and E should be doubled for a whole six-faced unit cell.

(hkl)†	$d(hkl)$ (Å)	V_{across}	V_{within}	E_{across} (kJ mol^{-1})	E_{within} (kJ mol^{-1})
(100)	56.4	2*A*	2*A*+4B+4C	587.7	1883.7
(010)	73.7	2*C*	4*A*+4*B*+2*C*	261.2	2210.2
(001)	30.4	4*B*+2*C*	4*A*+2*C*	1034.8	1436.6
(011)	28.1	4*B*+2*C*	4*A*+2*C*	1034.8	1436.6
(101)	26.8	2*A*+4*B*+2*C*	2*A*+2*C*	1622.5	848.9
(110)	44.8	2*A*	2*A*+4*B*+4*C*	596.0	1883.7

† Those planes having negative indices are equivalent to those with all positive indices.

low – since cooperative interactions is missing in one-dimensional objects to which steps belong. Therefore, correlation between the step rate and strength of the bonds parallel to the face remains a challenge. To the zeroth approximation, one may assume, in agreement with some measurements (see Chernov, 1989, 1993, and reference therein), that the step rates at similar supersaturations do not differ dramatically at various faces of the same crystal unless impurities are involved. Another unsolved problem associated with the application of the PBC is the unknown binding energies themselves, with respect not only to vacuum but especially relative to the energy that a growth unit acquires moving from the kink position to the mother solution or melt. The dependence of crystal habit on temperature comes mainly *via* temperature dependence of step propagation kinetics, *i.e. via* the activation energy. The 2D nucleation rate is also a function of temperature and is very sensitive to supersaturation, which dependencies are only implicitly within the PBC framework.

Another issue of classical molecular kinetic theory (Volmer, 1939) that has arisen recently especially in view of the atomic force microscope (AFM) capabilities is the kink concept and kink generation in complex structures. Since molecules are not equivalent within a unit cell, each molecule cannot be in a kink position: attachment and detachment of the molecule may change surface energy. In such lattices into which category the majority of substances fall, the steps and 'classical' Kossel kinks should be made of the whole unit cell: only detachment of the whole cell from the kink does not change the surface energy. The kinks made of the 7×7 cells revealed by scanning tunneling microscopy (STM) on the Si(111)–7×7 reconstructed face is a good example. This does not mean that the crystal grows by attachment of whole unit cells or their aggregates (though these aggregates may be present in solution in typically small amounts determined by thermodynamic conditions). What is present at the steps are only partly completed unit cells; Fig. 1 gives an example different to the Si(111)–7×7. Distribution of the molecular configuration should follow the Gibbs law. This distribution *via* configurational and vibrational entropies makes the chemical potential of all molecules at these kinks equal and, at equilibrium, equal to the chemical potential of a molecule in solution or other mother medium. We come to the conclusion that the molecular detachment energy should be averaged over the unit cell for the PBC analyses. Alternatively, to probe the crystal habit, one may operate with the energies needed to detach a unit cell as a whole. Again, it does not mean that the cell is a real building block actually involved in crystal growth. In §2.2, we apply, as an example, the PBC concept to the orthorhombic lysozyme shape.

2.2. *PBC geometry and energetics (orthorhombic lysozyme) (Oki et al., 1998)*

Application of the PBC needs to quantify various types of binding (Frey *et al.*, 1991). To determine periodic bond chains that are responsible for the habit of biocrystals, it is natural to first identify the bonds making contact between the molecules. In the refined structure of the orthorhombic lysozyme, three types of contacts, *A*, *B*, *C*, have been found (Oki *et al.*, 1998), making use of the program by Matsuura *et al.* (1979) that indicates the distances between atoms in neighboring molecules to be less that 4 Å (shorter distances might be chosen as well). The centers of *A*, *B* and *C* contacts on each molecule were connected with the centers of the neighboring molecules, as shown in the stereopair in Fig. 2. Red, yellow and blue lines correspond to the *A*, *B* and *C* contacts, respectively. Each molecule has six contacts with its neighbors, 2*A*, 2*B* and 2*C*. Correspondingly, each point in Fig. 2 from which six lines of three different colors emerge is the center of a molecule. The network of the strongest bonds obtained that way allows one to select the crystallographic planes expected on the crystal habit. The strength of each of the contacts, *A*, *B*, *C*, was estimated by counting the number of direct bonds between amino-acid residue atoms, water-mediated and assumed van der Waals bonds in the contact and ascribing to these bonds the energies of 12.56, 6.3 and 1.25 kJ mol^{-1}, respectively, following the estimates given by Kabash & Sander (1983), Frey *et al.* (1991) and Reid *et al.* (1985). These estimates give for the contacts

A, B and C the energies (with respect to vacuum) of 294, 193 and 13 kJ mol^{-1}, respectively. A straightforward way to test the importance of a face in a crystal habit is to determine the total energy of bonds of all chains running within the one-lattice-spacing-thick slice parallel to a face under consideration and to compare the result with the other faces. The number of chains that cross the planes restricting a unit cell and run on average parallel to the face under consideration is usually designated as V_{within}. The number of chains crossing the unit-cell top and bottom (parallel to the face) is associated with the detachment energy of the unit cell and designated as V_{across}. The total contact balance is

$$V_{\text{total}} = V_{\text{within}} + V_{\text{across}} = 4A + 4B + 4C, \qquad (1)$$

since there are 4 molecules in the unit cell. The face parallel to the strongest network, *i.e.* corresponding to the largest V_{within}, is the one with the smallest V_{across}. The result of the contact counting and corresponding energies, E, is listed in Table 1. The last column allows a judgment on the face importance in the crystal habit. These are the bond energies with respect to vacuum, rather than to the solution. The energies themselves have been estimated very roughly. We should also take into account fundamental inaccuracies associated with the PBC approach discussed above. Therefore, only major faces of the habit might be found.

Actual orthorhombic lysozyme crystals are faceted by large prismatic $(1\bar{1}0)$ (110) (1884 kJ mol^{-1}) and smaller (010) (2177 kJ mol^{-1}) faces covered by the $(0\bar{1}i)$ and (011) faces of lower E_{within} (1432 kJ mol^{-1}). The (101) faces were not observed, in agreement with 850 kcal mol^{-1} in Table 1. Discrepancies between Table 1 and the observed habit with respect to the importance of (110) and (010) faces seem to be within the accuracy of the approach and the approximations made.

Generally speaking, the energy V_{within} does depend on the shape of the unit cell(s) chosen for counting the number of broken contacts. If the face rate is determined by 2D nucleation, equilibrium shape of the nuclei should be chosen for the counting rather than the unit cell. This is an additional PBC simplification used in this example.

In conclusion, the PBC approach, though very efficient, should be supported by approaches taking into account energetics, specific growth mechanisms and kinetics.

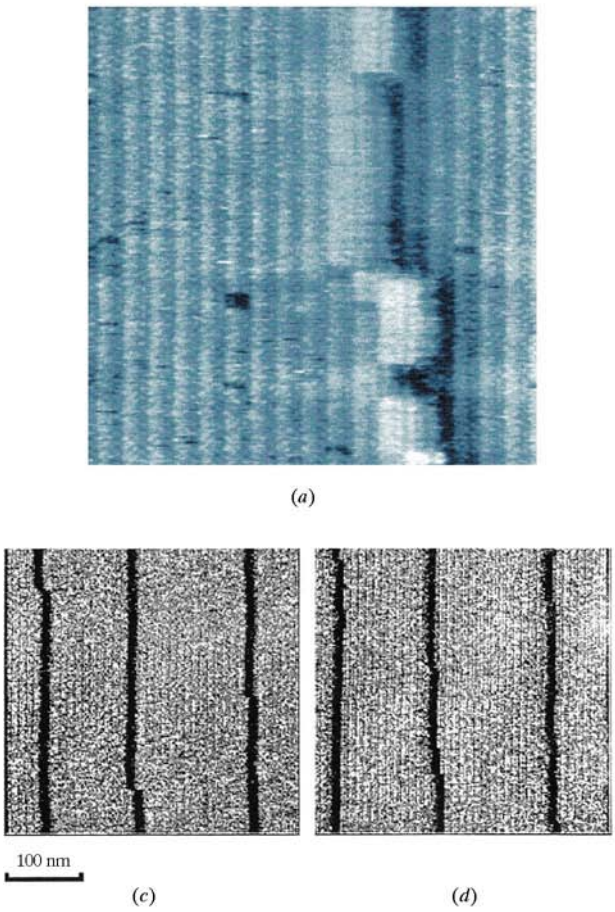

Fig. 1. AFM molecular resolution picture of the {011} thaumatin face. The growth step moves to the right *via* trangential motion of kinks up and down. The time difference between (*a*) and (*b*) is 2 min, with a scanning rate of 1 min frame^{-1}; (*a*) was scanned from top to bottom and (*b*) from bottom to top. The last molecular row forming the step is wider and narrower at different step portions showing that the complete unit cell (8 molecules) is not built at once. The wider row includes 8 molecules, the narrower row 6 molecules (Kuznetsov & Malkin, 1997). (*c*), (*d*) AFM images of low-kink-density steps on the (010) face of the orthorhombic lysozyme crystal moving to the left in the [100] direction. The time interval between frames is 51 s. The frame size is 385 × 385 nm (Rashkovich *et al.*, 1998). Courtesy of L. Rashkovich.

Table 2. *Surface energies of proteins*

1 erg cm^{-2} = 10^{-3} N m^{-1} = 1 mJ m^{-2}.

Protein	M (kDa)	$2R$ (nm)	ω (cm^3)	α (erg cm^{-2})	$\alpha\omega^{2/3}/kT$	Nucleus type	References
Insulin	7.3	2.7†	2×10^{-20}	0.5†	2.76	2D	(*a*)
Lysozyme	14.3	3.4	3×10^{-20}	1.2	1.26,‡ 2.3	2D	(*b*), (*c*)
Pumpkin globulin	112	5–6	1.5×10^{-19}	6.1×10^{-2}	0.43	3D	(*d*)
Apoferritin, ferritin	443	11–12	1.8×10^{-18}	2.7×10^{-2}	1.0	3D	(*d*)
STMV	1500	16–17	3.5×10^{-18}	1.8×10^{-2}	1.0	3D	(*d*)
Thaumatin	22	4	6.5×10^{-20}	0.4	1.6	2D	(*e*)
Canavalin	147	9–4	4.1×10^{-19}	0.6	8.3	2D	(*f*)
Catalase	250	4.2	7.2×10^{-20}	0.32	4.3	2D	(*g*)

† Found from ω assuming dimers as growth units. ‡ The surface per molecule on the ⟨110⟩ steps riser on the (110) face, 28×14 Å^2 = 4×10^{-18} m^2, was used instead of $\omega^{2/3} = 10^{-17}$ m^2. References: (*a*) Fiddis *et al.* (1979); (*b*) Chernov *et al.* (1995); (*c*) Durbin & Feher (1986); (*d*) Malkin & McPherson, (1994); (*e*) Malkin *et al.* (1996); (*f*) Land *et al.* (1995); (*g*) Malkin *et al.* (1998).

2.3. *Kinetics: inorganic vs protein crystals*

Application of *in situ* X-ray topography, Michaelson laser interferometry (Rashkovich, 1991; Chernov, 1989, 1993) and AFM (DeYoreo *et al.*, 1994, 1997) provided quantitative data on dislocation activity, kinetics of step propagation and the two most fundamental parameters of layerwise growth kinetics, *i.e.* effective step energy $\alpha = \alpha_l/h$ and step kinetic coefficient, β_{st}. Here, α_l is the actually measured linear free step energy and h is the step height. The step rate is related to β_{st} by the relationship

$$v = \beta_{st}\omega(C - C_e) = \beta_{st}\omega C_e[\exp(\Delta\mu/kT) - 1], \quad (2)$$

where C and C_e are the actual and equilibrium concentrations of solution and ω is specific molecular volume in the crystal. The face rate

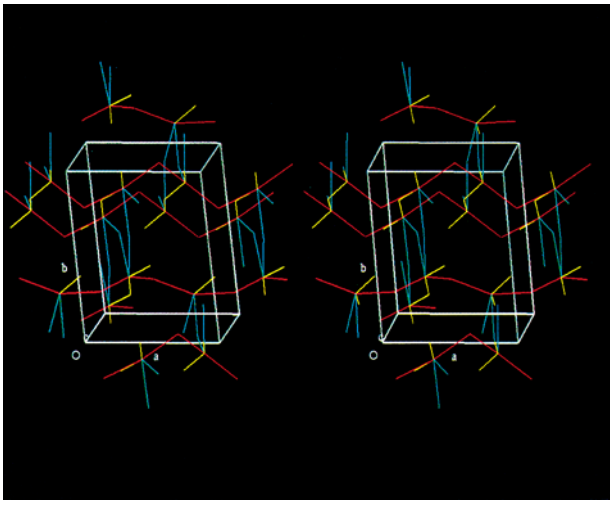

Fig. 2. Stereographic pair showing periodic bond chains connecting *A* (red), *B* (yellow) and *C* (blue) intermolecular contacts *via* the centers of the contacting molecules. These centers are the points at which three lines of each color meet. Each molecule has 6 neighbors, *i.e.* 2*A*, 2*B*, 2*C* contacts (Oki *et al.*, 1998).

$$V = pv, \quad (3)$$

where the local vicinal slope p is the (local) step density times step height, h. In the dislocation-controlled growth, p is just the slope of dislocation hillock and rises with supersaturation Typically, $p \simeq 10^{-3}$–10^{-2}. Therefore,

$$V = p\beta_{st}\omega(C - C_e), \quad (4)$$

so that $p\beta_{st}$ is the kinetic coefficient of the face. In many cases, p depends on supersaturation which makes $V(C - C_e)$ dependence nonlinear.

It is now well established that protein and inorganic crystals grow from solution by the same mechanisms of step generation by 2D nucleation and screw dislocation and subsequent step propagation along the face (Vekilov *et al.*, 1993; Kuznetsov *et al.*, 1995; Land *et al.*, 1995, 1997; Malkin *et al.*, 1996; Rosenberger *et al.*, 1996; Chernov & Komatsu, 1995; Chernov, 1997*a*). The difference between inorganic and protein crystals comes from their parameters. Effective free energies, α, of the step risers at the crystal–solution interface are summarized in Table 2.

Table 3 provides data on kinetic coefficients and hillock slopes (for the screw dislocation growth mode). The supersaturations used are also different: $\Delta\mu/kT$ = 0.001–0.002 for conventional, 0.1–0.2 for fast growth technologies of inorganic salts (*e.g.* KH_2PO_4 for laser frequency multiplication) *vs* $\Delta\mu/kT$ = 1–5 for protein crystallization. The purity level of solution reaches 10^{-5} for fast growth of inorganic salts while the 99% pure protein solution, *i.e.* 10^{-2}, is considered as ultrapure.

Absolute figures for α (Table 2) of the inorganic salt/solution interface exceed by two orders of magnitude those for proteins. However, the energies per one molecular site, *i.e.* $\alpha\omega^{2/3}$ (where $\omega^{2/3}$ is the typical area for one molecule) are very close. The same scaling is valid for the Young modulus, E: for inorganics, $E \simeq 10^{12}$ erg cm^{-3} while, for proteins, $E \simeq 10^{10}$ erg cm^{-3} (or dyn cm^{-2}). However, the stiffness per molecular contact, $E\omega^{2/3} \simeq 10^3$ dyn for both groups of crystals

Table 3. *Kinetic coefficients β_{st} of steps and vicinal slopes p*

Substance	Face	M (Da)	β_{st} (cm s^{-1})	p	$p\beta_{st}$ (cm s^{-1})	References
ADP, KDP, DKDP, $NH_4H_2PO_4$, KH_2PO_4	(100)		$(5–12) \times 10^{-2}$	3×10^{-4}–8×10^{-3}	10^{-4}–10^{-3}	(*a*), (*b*)
ADP	(101)		0.4	10^{-4}–5×10^{-3}	4×10^{-5}–5×10^{-3}	(*a*), (*b*)
$BaNO_3$	(111)		1.3×10^{-2}	$(3–15) \times 10^{-4}$	4×10^{-6}–2×10^{-5}	(*a*), (*b*)
$KAl(SO_4)_2 \cdot 12H_2O$ alums	(111)		8×10^{-2}	$(0.4–3.5) \times 10^{-3}$	3×10^{-5}–3×10^{-4}	(*a*), (*b*)
$Y_3Fe_5O_{12}$	(110), (211)			$(0.3–3) \times 10^{-2}$	$(0.4–1) \times 10^{-3}$	(*a*), (*b*)
$(YSm)_3(FeGa)_5O_{12}$	(111)		1.4×10^{-2}		10^{-2}	(*a*), (*b*)
$(EuYb)_3Fe_5O_{12}$	(111)				$(0.1–3) \times 10^{-3}$	(*a*), (*b*)
Lysozyme	(101)	14 300	4.6×10^{-5}	$(1.1–1.5) \times 10^{-2}$	6×10^{-7}	(*c*)
Canavalin		147 000	9×10^{-4}	9×10^{-3}	9×10^{-6}	(*d*),(*e*)
Thaumatin		22 000	2×10^{-4}	2D nucleation		(*f*)
Catalase		25 000	3.2×10^{-5}	2D nucleation		(*g*)

References: (*a*) Chernov (1992); (*b*)Vekilov *et al.* (1992); (*c*) Vekilov *et al.* (1993); (*d*) Kuznetsov *et al.* (1995); (*e*) Land *et al.* (1997); (*f*) Malkin *et al.* (1996); (*g*) Malkin *et al.* (1998).

(Chernov & Komatsu, 1995; Chernov, 1997*a*,*b*). Thus, the difference comes, in the first place, from the larger size of protein molecules while the bond strength is of the same order of magnitude. Indeed, the independently estimated contact strength for orthorhombic lysozyme (§2.2) of 293–125 kJ mol^{-1} with respect to vacuum is of the same class as *e.g.* metal and inorganic salt evaporation, 167–335 kJ mol^{-1}.

What makes a difference in growth kinetics, namely the much slower growth of protein crystals, is the rate of incorporation of molecules into the lattice, *i.e.* the step kinetic coefficient (Table 3). This difference also comes from the larger size of protein molecules *via* the high rotational entropic barrier for crystallization. Indeed, the probability that an asymmetric molecule arrives at a kink site in a proper orientation with respect to the lattice may be approximated by the steric angle within which a director of the molecule should remain for correct docking. This angle is the ratio between the squared radius of intermolecular forces, say 2–3 Å, to the squared effective molecular radius, say 20–30 Å. The ratio of these squares is 10^{-2}, which is a good proportion of the difference in the incorporation rate, *i.e.* in the kinetic coefficient, β_{st} (Table 3).

The dramatically higher supersaturations needed to grow protein compared to inorganic crystals suggest another essential difference in growth mechanism. It is known that the inverse supersaturation, $kT/\Delta\mu$, is a measure of relative excess of the incoming Brownian molecular flux to the kink sites over the opposite, outcoming, flux. For protein crystallization, $kT/\Delta\mu \simeq 1$ to 0.2 are typical. Thus, there is essentially no or only weak outcoming flux and therefore selection of species by the lattice *via* attachment of these species to the kink and preferential detachment of those of the wrong type (impurity or irregular species) or orientation. For comparison, during industrial silicon growth from the melt, $kT/\Delta\mu \simeq 10^5$; for solution growth at 2% supersaturation, $kT/\Delta\mu = 50$. We are therefore forced to conclude that selection of molecules possessing the right conformation, orientation and binding to continue a perfect lattice does not occur *via* the trial-and-error process typical of inorganics. Selection in protein growth occurs at the pre-kink level probably controlled by the tails of the Debye screened electrostatic potentials of the molecule, kink and surface sites. The latter may be important if adsorbed molecules are trapped by a preceeding step. Though these tail interaction energies do not exceed kT, they are able to perform a good selection as can be judged from the rocking-curve widths of tens of seconds and even less. Protein crystal perfection is discussed in §5.2.

2.4. *Step configurations*

Theory typically assumes that kink density is high at a step since this is a one-dimensional object without cooperative interaction and thus with intensive fluctuations. However, at a high kink energy/kT ratio, the density of kinks may be very low (compared to the lattice sites) so that the step is straight and does not meander. This happens *e.g.* for silicon at low temperature (Voronkov, 1973). AFM images of the steps parallel to the [001] direction on the (010) faces of orthorhombic lysozyme and the (011) face of thaumatin are shown in Fig. 1(*c*), (*d*). The average interkink distance for lysozyme is 4.5×10^{-3} nm^{-1} (Rashkovich *et al.*, 1998). Similar straight steps have been observed for calcite (DeYoreo, 1998). Under these conditions, the kinks appear through growth-induced one-dimensional nucleation only (Voronkov, 1973; Chernov, 1998*a*,*b*). In other words, from observations, the kink pairs do not appear *via* detachment of a unit cell (or part of it) from the straight step. Only one-dimensional growth nucleation occurs. Therefore, under practical growth conditions, kink nucleation, spreading along the step and annihilation occur at a rate exceeding the cell detachment rate so that equilibrium fluctuations are unable to develop. This may affect the action of the Gibbs–Thomson law for propagation of steps that are straight

and sufficiently short, *i.e.* containing only a few kinks. Let us consider a square-shaped island surrounded by such a kink-free step. Let the square side length, l, be comparable with the equilibrium length, $\omega\alpha/\Delta\mu$. The Gibbs–Thomson dependence of the supersaturation which drives the expansion of the small square island is

$$\Delta\mu' = \Delta\mu - \omega\alpha/l. \quad (5)$$

However, the kink pairs (one-dimensional nuclei) appear on the island edges at any place by random attachments and detachments of species. These events and, thus, the one-dimensional nucleation probability do not depend on the step length because the new-born kinks 'do not know' about the corners, since the molecular interaction potential scale is small compared to l. Therefore, the propagation rate of the short step under these conditions will not depend on its length, *i.e.* the rate will not obey the law given by (2) with $\Delta\mu$ replaced by $\Delta\mu'$ from (5). Such 'violation' of the Gibbs–Thomson law by kinetics may happen only if a kink split from one of the step ends is unable to reach the opposite end. In other words, the fluctuation of the step shape at which the Gibbs–Thomson law operates is missing at sufficiently high supersaturation.

2.5. *Atomic structure of interfaces*

STM, AFM and X-ray diffraction techniques in recent years have helped to answer in some cases a long-standing question: what are the actual species that form the last lattice layer exposed to the mother liquor or the crystal–vacuum interface? This question is not trivial for all complex lattices whose structure, within a one-lattice-spacing-thick layer, includes several different molecular layers parallel to the major faces. The simplest example is *A* and *B* faces of III–V or II–VI semiconductors. Low-energy electron diffraction (LEED) and reflection high-energy electron diffraction (RHEED) have been used for some time. At the crystal–solution interface, grazing-angle incidence diffraction and crystal truncation-rod techniques were used (Robinson, 1986; Feidenhans'l, 1989; Gidalevitz, Feidenhans'l, Smilgies & Leiserowitz, 1997; De Vries *et al.*, 1998).

Solution of the problem is important in order to construct a molecular picture of growth and to be able to judge the impurity, solute and solvent adsorption on these faces. Amino acid α-glycine and β-alanine crystals are used as examples (Gidalevitz, Feidenhans'l & Leiserowitz, 1997). In the former, there is a choice between the (010) surfaces terminated by either the CH_2 groups or those exposing CO_2^- and NH_3^+ groups to solution. Within the crystal, the CH_2-exposing layers are van der Waals bonded while the layers exposing CO_2^- and NH_3^+ groups are bonded by the corresponding hydrogen bonds. The intensity of diffuse grazing-angle X-ray scattering in the vicinity of Bragg peaks and between the truncation rods was used. It was found that the more hydrophobic CH_2 groups are actually exposed both to the air, when the cleavage surface was investigated, and to aqueous solution when these (010) surfaces grew or dissolved. The preferential cleavage through van der Waals contacts rather than through the stronger hydrogen bonding is quite natural. The exposure of hydrophobic CH_2 groups rather than hydrophilic carboxyl and amino groups to solution suggests that the solvation energy gain is smaller than the gain due to crystallization. Knowledge of the actual atomic structure of the interface explains why (*S*)-methionine chose the $(0\bar{1}0)$ face of α-glycine to be preferably adsorbed – it makes hydrogen bonds, poisons the face and decreases the growth rate.

The similar problem of lattice termination was solved by the same truncation-rod-intensity analysis of the dipyramidal {101} faces of KH_2PO_4, which may be terminated by either K^+ or $H_2PO_4^-$ groups (De Vries *et al.*, 1998). It was shown that K^+ ions are sitting on the {101} terraces explaining why cations (*e.g.* Cr^{3+}, Fe^{3+}, Al^{3+}) do not influence the bipyramidal faces while they can decrease the rate of the prismatic {010} face build up of alternating positive and negative ions.

3. Non-faceted growth: disordered surfaces

Introduction of binding energies into the geometric approach means that the influence of temperature on the growth mode can be taken into account. Indeed, the dimensionless ratio $2\varepsilon/kT$ measures in kT units the energy 2ε needed to create a step (per unit site), *i.e.* the energy ε of a bond 'dangling' mainly 'parallel' to the face on which the step separates the completed and non-assigned portions of the next layer. The smaller ε/kT, the more intensive is the configurational fluctuation of the step and thus the higher its entropy, s, and the lower is the step free energy, $\alpha_l a = \varepsilon - Ts$, where a is the length of the unit site along the step and s is the configurational entropy of the step. At a critical ε/kT ratio, $(\varepsilon/kT)_c$, the step energy vanishes and becomes negative at higher temperatures, $T > T_c$, and/or lower step potential energy ε. If the step free energy α_l becomes negative, the system favors maximal elongation of steps to decrease its total free energy. Such elongation happens by splitting the surface molecular layer into microscopic molecular-sized islands so that the step disappears. In other words, the fully completed lattice surface layer limited by the step intermixes with the uncompleted (empty) two-dimensional space on the opposite side of the step. Ultimately, the surface becomes rough containing adatoms and their clusters with the kink-like configurations homogeneously distributed throughout the face. This roughening concept introduced in the 1940s explains why metals and other substances possessing low entropy of phase transition $\Delta s < \sim(1\div2)k$ do not show facets. Indeed, lower transition entropy means low heat of transition and thus

low ε/kT. Since at the rough surface the step energy is zero or less, kinks are homogeneously spread over the surface and cooperative interaction is destroyed by temperature and the two-dimensional nucleation is not needed to generate steps and thus kinks. Therefore, the face growth rate is proportional to the low driving force for crystallization:

$$V = \beta\omega C_e \Delta\mu/kT = \beta_\mu \Delta\mu/kT. \tag{6}$$

If the mother liquor is a melt, $\omega C_e \simeq 1$. For growth from solutions, ωC_e is essentially a solubility relative to water-free crystal and varies from 0.2–0.5 for well soluble to 10^{-3}–10^{-5} or less for poorly soluble slats, like calcium phosphates, carbonates and minerals in living nature.

For melt growth, the definition (6) of β (cm s^{-1}) is often replaced by the experimentally more convenient coefficient β^T (cm s^{-1} K^{-1}) connecting the growth rate and supercooling, ΔT, at the interface:

$$V = \beta^T \Delta T \tag{7}$$

$$\beta^T = \beta_\mu \Delta s/kT, \tag{8}$$

where Δs is the entropy of fusion. The kinetic coefficient β in (6) is slightly (several times rather than orders of magnitude) smaller than the step kinetic coefficient β_{st} in (2) because it essentially presents the rate of incorporation of species at the kink whose density is assumed to be high on both steps [equation (2)] and rough surfaces [equation (6)]. For instance, for Si, $\beta^T \simeq 20$ cm s^{-1} K^{-1} or, with $\Delta s \simeq 5k$, $T = 1670$ K, $\beta_\mu \cong 7 \times 10^3$ cm s^{-1}. This is about five orders of magnitude larger than the step kinetic coefficient for inorganic solution growth. The reasons are in lower, if at all present, potential and entropic barriers to crystallization from a simple melt, compared to solution growth. The difference in growth rates between the layerwise growing face and a rough step or surface is even more dramatic.

Since the rough interface possesses a very high kinetic coefficient, it needs much lower supercooling or supersaturation to grow at the same rate as a facet. *E.g.* for Si, the (111) face grows at $\Delta T \simeq 0.5$ K, while for the rough interface a ΔT of only $\sim$0.01 K is needed. Because of the low driving force needed, the rough surface follows just the melting-point isotherm (or, in general, the surface at which the temperature and concentration equilibrium is achieved).

Introducing the roughening concept, we operate with the critical ε/kT ratio, implicitly assuming the 'dangling bond' energy ε, *i.e.* that an atom or a molecule belongs either to the crystal or to the melt (the lattice liquid model). This is a very productive method for calculations and Monte-Carlo simulations. Since the crystal–liquid surface in this model is strictly localized, the phases are assumed to be different by interaction energies only [we ignore the model that assumes spreading of the interface with respect to energies, keeping the lattice liquid approximation intact (Bennema, 1996)]. The way to get rid of the lattice model is to present a liquid as a combination of density waves using, for approximation, the same set of reciprocal-lattice vectors as the real crystal. Making use of this approach, we may consider simultaneous building of several lattice planes parallel to the interface under consideration, as is shown in Fig. 3. The basic equation to find the kinetic coefficient is the balance of energy dissipation within the transient position disordered liquid layer (Mikheev & Chernov, 1991):

$$(kT/2)\sum_{\mathbf{G}} \int |j_{\mathbf{G}}|^2 D_{\mathbf{G}} n \, dz = nV\Delta\mu. \tag{9}$$

Here the dissipation on the left-hand side comes from diffusion flexes $j_{\mathbf{G}}$ ordering atoms into the density waves with the wave vectors $\mathbf{G}$ *via* diffusivities $D_{\mathbf{G}}$. Integration is over all the transition layer, as is shown in the upper part of Fig. 3. The number density n of species is supposed to be equal in the crystal and liquid. To evaluate the diffusivities, *i.e.* typical frequencies corresponding to different density waves, the experimental correlation between the static and dynamic structure factors was employed (Cohen *et al.*, 1987). The final expression for the kinetic coefficient includes the static structure factor, the typical frequency is proportional to the thermal gaseous velocity of the particles of mass m, $(kT/m)^{1/2}$. It contains also the factor depending on the

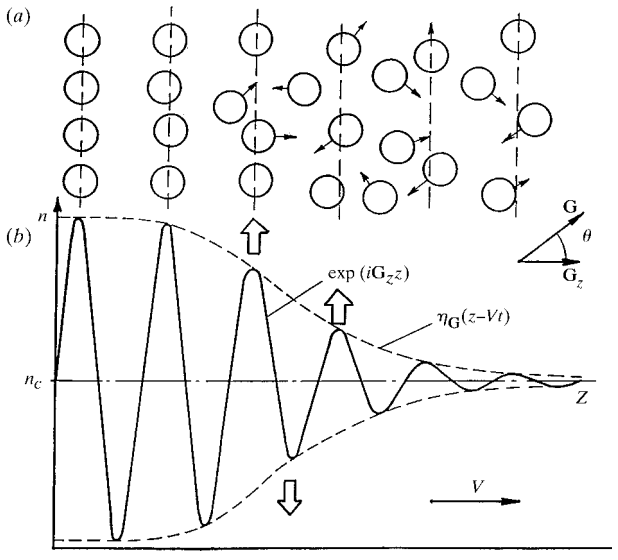

Fig. 3. Density waves in an ordered crystal (left) decrease their amplitudes owing to continuous disordering at the interface with the melt (right). The crystallization process means ordering the atoms by moving them towards their positions in atomic planes, as shown by arrows in (*a*). Correspondingly, the amplitude of each density wave rises, as shown by the bold arrows in (*b*). $\mathbf{G_z}$ is normal to the face while $\mathbf{G}$ is a reciprocal-lattice vector of an arbitrary density wave. V is the face growth rate, t is time, the coordinate x is normal to the face. The envelope $\eta_{\mathbf{G}}(z - Vt)$ of the density wave serves as the order parameter (*cf.* Mikheev & Chernov, 1991).

angles between the normal to the interface under consideration and the major reciprocal-lattice vectors. There is no potential barrier for crystallization in this case, contrary to the classical equation and in agreement with some experimental evidence (Ovsienko & Alfintsev, 1980). We thus come to the conclusion that continuous transition between the lattice and disordered melt may occur *via* simultaneous ordering of several layers within the rough interface spread over several lattice spacings.

4. Subsurface ordering of liquids

Liquid near a solid wall should be ordered just because the first atomic liquid layer is attached to the wall and the next layers inherit part of this ordering. Correspondingly, smectic-like and more general density waves corresponding to various reciprocal-lattice vector directions should be induced in the liquid by a crystal surface (Mikheev & Chernov, 1987). Such ordering has been confirmed by X-ray diffraction from liquid gallium on the (111) diamond surface (Fig. 4) (Huisman *et al.*, 1997). Another confirmation comes from measurement of the force acting on the AFM tip approaching highly oriented pyrolytic graphite and a mica cleavage surface (Fig. 5).

Similar subsurface ordering at the interface between a crystal and its own melt has not been experimentally reported so far. Therefore, there remains two possibilities for the rough crystal–melt interface. One is the meandering in time and space of the strictly localized interface dividing 'solid' and 'liquid' species according to the lattice model of a liquid. Another is a real continuous positional disordering associated with the surface-induced density waves, as demonstrated in Figs. 4 and 5. This is not a trivial choice since meandering of a localized interface might be reduced to the similar density waves. However, the lattice model would not explain the change in the structure of density waves near different faces obtained by molecular dynamics simulations (Bonnisent, 1983).

5. Perfection of crystals

Various optical and X-ray diffraction studies of grown crystals have always been a major part of crystal growing. These crystal characterization facilities are associated with any crystal growth laboratory along with X-ray and electron micropole analyses of crystal composition inhomogeneities and other techniques. These crystallographic tools provide deep diagnostics of crystal defects attributed to crystal-growth processes.

High-precision composition and ordering analyses of mixed single-crystalline phases is another area of structure–growth interrelation. For instance, diffraction analyses of fluorite solid electrolytes allow one to predict the compositions needed to achieve required electric conductivity and to control the correspondingly grown crystals (Simonov, 1992; Grigor'eva *et al.*, 1996; Zhurova *et al.*, 1996).

5.1. *Origin of defects*

The origin of defects remains a major issue of crystal-growth science and technology and is associated with the linkage of several groups of phenomena as follows.

Surface phenomena like adsorption and subsequent nonequilibrium trapping of impurities, vacancies, variations of stoichiometry in II–VI and III–V compounds, antisite defects in III–V compound semiconductors grown from molecular beams, vapor, melt or solution cause defects. If a crystal grows with facets, these defects typically produce different concentrations in different growth pyramids, the material of which was formed by different crystallographic faces. In such crystals, the point-defect distribution is never the equilibrium one. Even steps possessing different orientations on the same face produce material with different amounts of point defects and vicinal sectoriality appears (Smol'skii *et al.*, 1984).

Transport phenomena in mother melt or solutions are responsible for striations induced by convection and

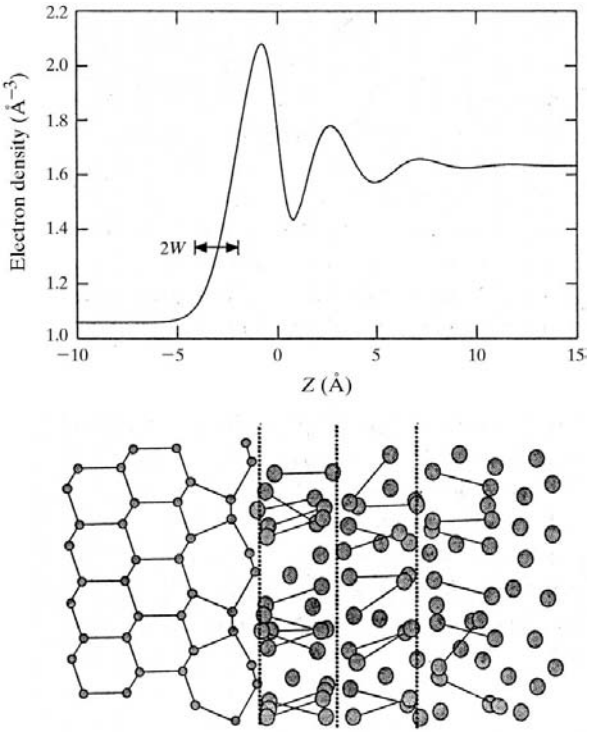

Fig. 4. Electron-density map of liquid Ga on the (111) face of diamond from X-ray diffraction data (upper panel). The lower panel shows the model of subsurface ordering of Ga on the left containing monomer and dimers (connected full circles) (Huisman *et al.*, 1997).

temperature fluctuations. Demand in understanding and ultimate elimination of these inhomogeneities initiated extensive studies of heat and mass transport, including the ones under microgravity conditions. These studies demonstrated the essential role of Maragoni convections, under both terrestrial and microgravity conditions. This convection is known to be driven by temperature and/or concentration gradients inducing gradients in surface tension along free liquid surfaces. Variation of residual gravity direction at a level as low as 10^{-6} g by various orientations of a space craft in orbit induce up to 10^{-1} scale variations of stoichiometry in *e.g.* CdHgTe crystals (Gillies *et al.*, 1997). Vibrations on the space craft, particularly manned ones, also induce crystal inhomogeneities. So do low-level accelerations when the space craft alters its orientation, not to mention the change of the orbit itself. Such extreme sensitivity of the crystal–melt interface and crystallizing system to transport rate gave rise to efforts aimed at suppressing convection with a magnetic field (Watring & Lehoczky, 1996). A magnetic field is already exploited to produce silicon crystals.

Instabilities of the growing interface initiated by random noise, *i.e.* spatial or temporal deviations of the original smooth-growing interface and developed at certain growth condition, especially by liquid flows and associated temperature fluctuations, cause defects. Such morphological instability happens when, *e.g.*, the mother melt is undercooled and the growing interface is rough (Coriell & McFadden, 1993). Morphological instability happens also on the layerwise growing interface. In this case, the interface does not grow by spreading of equidistant elementary steps of equal (lattice spacing high) height. Instead, these steps form bunches (Chernov, 1984). These bunches trap point defects in amounts depending on the bunch speed and height so that the grown crystals contain striae (Bauser, 1994). This kind of striation is essentially different from one caused by changes in conditions external to the surface processes, like convection-induced temperature and concentration variations. The step bunching is a result of interaction between steps *via* overlapping of diffusion fields surrounding each of the steps because each step is a sink for solute in solution growth, heat source in melt growth and sink or source of impurities. Therefore, striations induced by step bunching is a coupled surface–bulk transport phenomenon and occurs, like any instability, even under externally ideally constant temperature and concentration. The step bunching was found to be dependent on solution-flow direction relative to the step movement (Chernov *et al.*, 1986; Chernov, 1992; Coriell *et al.*, 1996, 1998). If both solution and steps are moving in the same direction, the bunching is dramatically enhanced. If the flows are antiparallel, the bunching is strongly suppressed. This flow-dependent effect of bunching was first discovered in $NH_4H_2PO_4$ (ADP) crystals (Chernov *et al.*, 1986) and confirmed on lysozyme (Vekilov *et al.*, 1996, 1997). In the latter case, the flow induced by solute convection (at a rate of *ca* 100 μm s^{-1}) was sufficient. The traces of the step bunches in the crystal were visible by optical contrast if viewed strictly parallel to the trace plane (Vekilov & Rosenberger, 1998).

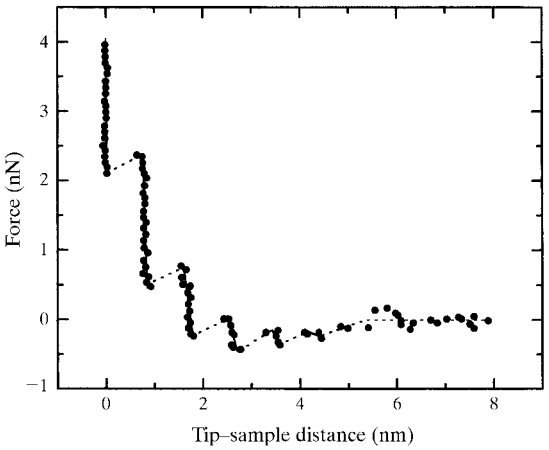

Fig. 5. Oscillations of the force acting on the AFM tip approaching a mica surface covered with *n*-dodecanal (Nakada *et al.*, 1996). Each force peak corresponds to piercing of a smectic-like liquid layer ordered by the mica surface at 298 K. At 313 K, the period of oscillation is doubled.

Post-crystallization evolution of defects, stress and strain distribution is typical of melt growth of, for example, elementary and compound semiconductors where point defects and dislocations are mobile. Therefore, perfection of these materials essentially depends on the temperature distribution. Inevitable annealing of the just grown portion of a crystal during the growth process itself or special annealing results in stress relaxation and reaction between the trapped impurities, like metal impurities and vacancies in the semiconductors remaining plastic in a wide range of temperature below their melting points. Thermal stress is induced by inhomogeneous distribution of temperature in a growing crystal. Therefore, the lower the heat conductivity the higher are the second derivatives of the temperature inducing this stress. This stress is relaxed by creation of dislocations, stacking faults and twins. The lower the energy needed to create these defects, the easier is stress relaxation during the growth and the higher may be the residual stress in the cooled crystal induced by these defects. In the sequence of Ge, Si, III–V, II–VI compounds, the thermal conductivity increases while the stacking-fault energy decreases. Therefore, growing perfect bulk crystals of elementary semiconductors is easier than the compound ones, especially the II–VI compounds. In these crystals, twinning may occur in the crystal bulk under the condition of high local stress as well as at favorable conditions on the growing crystal face.

5.2. *Defects in solution-grown crystals*

At least three groups of crystals growing from solution have attracted much attention in the last few years: large optically nonlinear crystals for frequency doubling, mainly KH_2PO_4 (KDP) and $KH_{2-x}D_xPO_2$ (DKDP); proteins and other biological compounds; and biominerals, like Ca phosphates and carbonates, oxalates and urates. For the first two categories of crystal, perfection is the major issue. For the KDP group, a high laser threshold is required in order to use these crystals in high-intensity laser beams and refractive-index homogeneity to reach phase matching for frequency multiplication (Bespalov *et al.*, 1987; DeYoreo *et al.*, 1995; Zaitseva *et al.*, 1997). Perfection of biocrystals is needed to reach high resolution in revealing the spatial structure and functions of the biomolecules of which these crystals are built. Striation and mosaicity seem to be the major established defects that cause deterioration of crystal quality. Fig. 6 presents an example of high-precision X-ray topography revealing mutual rotation between neighboring striation layers in KDP crystals. The rotation amplitude is *ca* 10^{-6} rad, *i.e.* less than a second angle range (Smol'sky *et al.*, 1996; Voloshin *et al.*, 1996, 1998). These crystals have been grown in the Lawrence Livermore Laboratory making use of reagents with a level of impurities less than 10^{-5}. On the other hand, it is well known that specific impurities induce splitting, mosaicity and lattice rotation in numerous crystals grown from solution (Lemmlein, 1973; Punin, 1981, 1983, 1994; Kuzmina *et al.*, 1987; Punin & Gorskaya, 1992; Punin & Ivanova, 1993; Shtukenberg *et al.*, 1993). These phenomena may be understood bearing in mind that a point defect in a crystal lattice is a source of internal stress and may be considered as an elementary stress center (Chernov, 1998*b*).

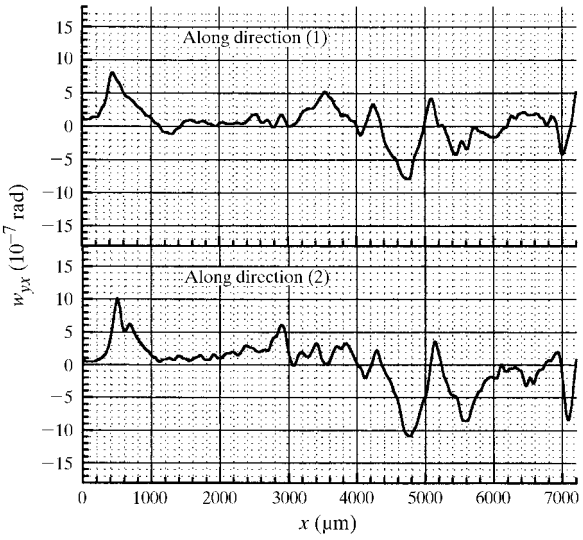

Fig. 6. Mutual rotations of lattice layers making striations parallel to the dipyramidal (101) KDP face measured along two cross sections (directions 1 and 2) normal to the face and the striation layers (Smol'sky *et al.*, 1996; Voloshin *et al.*, 1998).

Recent experiments showed that a covalently bound lysozyme dimer is the important impurity deteriorating crystal quality. These dimers are present at *ca* 0.5% in solution (Carter *et al.*, 1998). The distribution coefficient, K, of an impurity, *e.g.* of these dimers, at the growing interface may be introduced as

$$K = (n_{iS}/n_{pS})/(n_{iL}/n_{pL}), \tag{10}$$

where n is the number densities of regular protein (p) or impurity (i) species in the crystalline solid (S) and liquid (L) phases. In space, the impurity distribution around a crystal viewed as a sphere of radius R obeys the Laplace diffusion equation with the boundary condition

$$\begin{aligned} D_i \partial n_{iL}/\partial r &= (n_{iS} - n_{iL})V \\ &= [K(n_{pS}/n_{pL}) - 1]Vn_{iL} \\ &\equiv \beta_i n_{iL}. \end{aligned} \tag{11}$$

Here, D_i is the diffusivity of impurity, V is the crystal growth rate and $\partial/\partial r$ is the derivative operator normal to the crystal surface. Solution of the diffusion problem gives the experimentally measured effective distribution coefficient:

$$K_{\text{eff}} = (n_{iS}/n_{pS})/(n_{iL\infty}/n_{pL\infty}) = K/(1 + \beta_i R/D_i). \tag{12}$$

Opposite to K [equation (10)], K_{eff} is related to the measurable concentrations far away from the crystal, at $r = \infty$. If the impurity is preferentially trapped by the crystal, which is the case with covalent dimers, $\beta_i > 0$ and $K_{\text{eff}} < K$. This is because a zone depleted with respect to the impurity exists around the crystal. Taking for an estimate for the terrestrial convection assisted growth $K = K_{\text{eff}} = 9$, $V = 5 \times 10^{-8}\,\text{cm s}^{-1}$, $n_{pS}^{-1} = \omega = 3 \times 10^{-20}\,\text{cm}^{-3}$, $n_{pL} = 10^{18}\,\text{cm}^{-3}$ (lysozyme concentration of $25\,\text{g l}^{-1}$), $D_i = 7 \times 10^{-11}\,\text{m}^2\,\text{s}^{-1}$ and $R = 3 \times 10^{-4}\,\text{m}$, one has $\beta_i = 1.5 \times 10^{-7}\,\text{m s}^{-1}$ and $\beta_i R/D_i \simeq 0.6$. The latter figure means that the relative depletion is *ca* 60%, *i.e.* is of the order of magnitude of the concentration itself. For comparison, depletion with respect to regular protein molecules is only several percent. For crystals grown in space, K_{eff} was measured by dissolving the whole crystal of final radius R_f, *i.e.* by averaging (12) over $0 < R < R_f$. This $\langle K_{\text{eff}} \rangle = 2$, *i.e.* 4.5 times lower that on Earth where convection destroys the depleted zone. This lower concentration of impurity in the space-grown crystal should be the reason for its confirmed higher diffraction quality (Carter *et al.*, 1998). These data support our hypothesis (Chernov, 1997*a*,*b*; Vekilov & Rosenberger, 1998) that the microgravity-induced improvement of protein-crystal quality is associated with the lower amount of stress-inducing impurities trapped by the crystal. Elimination of this stress causes mosaicity dislocations and/or cracking. If the impurity is rejected by the growing crystal so that $\beta_i < 0$,

microgravity would have a negative effect on the crystal quality.

The mechanism of crystal deterioration by the trapped impurities is associated with the internal strain and stress tensor ε°_{lm} induced by each of the impurity species in the crystal lattice (Chernov, 1997*a*,*b*). The strain fields of these centers overlap, inducing macroscopic stress in the crystal (Khachaturyan, 1983):

$$\varepsilon_{lm} = \varepsilon^{\circ}_{lm} C. \tag{13}$$

Here C is the number of regular sites occupied by stress centers, relative to all regular sites in an ideal lattice. Equation (13) is equivalent to the thermal expansion equation, C playing the role of temperature and ε°_{lm} the role of thermal expansion tensor. It can be shown (Chernov, 1998*b*) that, if the center concentration in the neighboring striation layers parallel to the growing face differ by δC, the mutual lattice rotation, $\delta\omega$, occurs only around the axes x and y within the striation plane, $z = 0$:

$$\delta\omega_x = -\varepsilon^{\circ}_{yz}\delta C, \quad \delta\omega_y = \varepsilon^{\circ}_{xz}\delta C,$$
$$\delta\omega_z = (\varepsilon^{\circ}_{yz} - \varepsilon^{\circ}_{xy})\delta C = 0. \tag{14}$$

With $\delta C \simeq 10^{-2}$, *i.e.* 1% of impurity, and $\varepsilon^{\circ}_{lm} = 3 \times 10^{-2}$, as estimated for the given growth conditions, one may expect lattice rotation $\delta\omega \simeq 3 \times 10^{-4}$ rad $\simeq 1''$. The corresponding internal stress is $\sim G\varepsilon \simeq 3$ kg cm^{-2} = 3×10^5 Pa. Our first attempt to estimate the strength of monoclinic lysozyme crystals (Holmes *et al.*, 1998) give 0.5 kg cm^{-2} = 0.5×10^5 Pa. If this estimate is correct, then the strain of 3×10^{-4} cannot cause elastic stress: the crystal should either acquire mosaicity or crack. Further investigations of the different proteins, impurities and growth conditions are needed to confirm or reject the impurity-induced microgravity effect and corresponding recommendation on improvement of crystal quality under terrestrial growth conditions.

6. Conclusions

The relationship between crystal structure and growth morphology can be described by the PBC approach though quantitative data on binding energies and growth conditions should be introduced for more adequate analyses.

The kink concept for the complex lattices should be generalized. Fluctuations do not provide sufficient kink density on steps and therefore the Gibbs–Thomson relationship for straight steps may fail even at not very high supersaturations.

The lattice model of a melt may be replaced by the density-wave approach to evaluate the growth kinetic coefficient. More analysis is needed to determine if surface roughness is associated with continuous positional disordering of the species within the crystal–melt transition layer rather than with fluctuations of the sharp interface. However, X-ray diffraction, AFM data and molecular dynamic simulation provide more support for the positional disordering model.

Relating Young moduli and surface energies of protein crystals to area per molecule rather than per m^2 eliminates dramatic differences between figures for these parameters for protein and inorganic crystals. Nevertheless, orders-of-magnitude differences in the growth kinetic coefficient associated with large molecular size and asymmetry remain. Selection of proper species occurs on the pre-kink level rather than *via* trial-and-error processes that include incorporation into the lattice, as happens with inorganics.

Protein-crystal perfection is essentially determined by impurities inducing internal stress. The higher quality of crystals grown in microgravity seems to be associated with lower amounts of these impurities, like covalently bound dimers in tetragonal lysozyme. These preferentially trapped impurities have lower concentration in solution around crystals growing in microgravity and thus inside the crystals. In the presence of active impurities repelled by growing crystals, the crystals grown in space should have more defects and allow for lower structural resolution.

Many thanks to Ms S. Zarger for her help in preparing this manuscript. Support of NASA under Grants NAG8-1354 and 1454, and of LLNL under Agreement B304321 are gratefully acknowledged.

References

Bauser, E. (1994). *Handbook of Crystal Growth*, edited by D. T. J. Hurle, Vol. 3C, p. 879. Amsterdam: Elsevier.
Bennema, P. (1993). *Handbook of Crystal Growth*, edited by D. T. J. Hurle, Vol. 1A, pp. 477–581. Amsterdam: Elsevier.
Bennema, P. (1996). *J. Cryst. Growth*, **166**, 17–28.
Bespalov, V. I., Bredikhin, V. I., Katsman, V. I., Ershov, V. P. & Lavrov, L. A. (1987). *J. Cryst. Growth*, **82**, 776.
Bonnisent, A. (1983). *Crystal Growth, Properties and Applications*, Vol. 9, pp. 1–21. Berlin: Springer.
Carter, D. C., Lim, K., Ho, J. X., Wright, B. S., Twigg, P. D., Miller, T. Y., Chapman, J., Keeling, K., Ruble, J., Vekilov, P. G., Thomas, B. R., Rosenberger, F. & Chernov, A. A. (1998). *J. Cryst. Growth*. Submitted.
Chernov, A. A. (1984). *Modern Crystallography. III. Crystal Growth*. *Springer Series of the Solid State*, Vol. 36. Berlin: Springer.
Chernov, A. A. (1989). *Contemp. Phys.* pp. 251–276.
Chernov, A. A. (1992). *J. Cryst. Growth*, **118**, 333–347.
Chernov, A. A. (1993). *Prog. Cryst. Growth Charact.* **26**, 121–151.
Chernov, A. A. (1997*a*). *Phys. Rep.* **288**, 61–75.
Chernov, A.A. (1997*b*). *J. Cryst. Growth*, **174**, 354–361.
Chernov, A. A. (1998*a*). Proc. ISSCG10, 1–6 June 1998, Rimini, Italy.
Chernov, A. A. (1998*b*). *J. Cryst. Growth.* In the press.
Chernov, A. A. & Komatsu, H. (1995). *Science and Technology of Crystal Growth*, edited by J. P. van der Eerden & O. S. L. Bruinsma, pp. 67–80, 327–353. Dordrecht: Kluwer Academic Publishers.

Chernov, A. A., Kuznetsov, Y. G., Smol'sky, I. L. & Rozhansky, V. N. (1986). *Sov. Phys. Crystallogr.* **31** 705–712.
Chernov, A. A., Pusey, M. l., Forsythe, E. L. (1995). Abstracts, ICCBM, Hiroshima, November 1995, p. 48.
Cohen, E. G. D., Westerhuijs, P. & de Schepper, T. M. (1987). *Phys. Rev. Lett.* **59**, 2872–2874.
Coriell, S. R. & McFadden, G. B. (1993). *Handbook of Crystal Growth*, edited by D. T. J. Hurle, Vol. 1B, p. 783. Amsterdam: Elsevier.
Coriell, S. R., Murray, B. T., Chernov, A. A. & McFadden, G. B. (1996). *J. Cryst. Growth*, **169**, 773–785.
Coriell, S. R., Murray, B. T., Chernov, A. A. & McFadden, G. B. (1998). *J. Cryst. Growth*, **183**, 669–682.
De Vries, S. A., Goedtkind, P., Bennett, S. L., Huisman, W. J., Zwanenburg, M. J., Smilgies, D. M., DeYoreo, J. J., van Enkevort, W. J. P., Bennema, P. & Vlieg, E. (1998). *Phys. Rev. Lett.* **80**, 227–231.
DeYoreo, J. J. (1998). Private communication.
DeYoreo, J. J., Land, T. A. & Daiz, B. (1994). *Phys. Rev. Lett.* **73**, 838–841.
DeYoreo, J. J., Land, T. A., Rashkovich, L. N., Onischenko, T. A., Lee, J. D., Monovskii, O. V. & Zaitseva, N. P. (1997). *J. Cryst. Growth*, **182,** 442–460.
DeYoreo, J. J., Rek, Z. V., Zaitseva, N. P. & Woods, B. W. (1995). *J. Cryst. Growth*, **166**, 291–297.
Durbin, S. D. & Feher, G. (1986). *J. Cryst. Growth*, **76**, 583.
Feidenhans'l, R. (1989). *Surf. Sci. Rep.* **10**, 105–188.
Fiddis, R. W., Longman, R. A., Calvert, P. D. (1979). *J. Chem. Soc. Faraday Trans. I*, **75**, 2753–2761
Frey, M., Genovesio-Taverne, J.-C. & Fontecilla-Camps, J. C. F. (1991). *J. Phys. D*, **24**, 105–110.
Gidalevitz, G., Feidenhans'l, R. & Leiserowitz, L. (1997). *Angew. Chem.* **36**, 959–962.
Gidalevitz, D., Feidenhans'l, R., Smilgies, D. M. & Leiserowitz, L. (1997). *Surf. Sci. Lett.* **4**, 721–932.
Gillies, D. C., Lehoczky, S. L., Szofran, F. R., Watring, D. A., Alexander, H. A. & Jerom, G. A. (1997). *J. Cryst. Growth*, **174**, 101–107.
Grigor'eva, N. B., Otroshchenko, L. P., Maximov, B. A., Zhurova, E. A., Sobolev, B. P. & Simonov, V. I. (1996). *Crystallogr. Rep.* **41**, 51–55.
Hartman, P. (1973). *Crystal Growth. An Introduction*, edited by P. Hartman, pp. 367–402. Amsterdam: North Holland.
Holmes, A. M., Witherow, W. K. & Chernov, A. A. (1998). Unpublished results.
Huisman, W. J., Peters, J. F., Zwanenburg, M. J., De Vries, S. A., Derry, T. E., Abernathy, D. & van der Veen, J. F. (1997). *Nature (London)*, **290**, 379–381.
Kabash, W. & Sander, C. (1983). *Biopolymers*, **22**, 2577–2637.
Khachaturyan, A. G. (1983). *Theory of Structured Transformations in Solids.* New York/Chichester: John Wiley.
Kuzmina, M. A., Punin, Y. O. & Kamentsev, U. E. (1987). *Zapiski Vses. Mineral. Obsh.* **116**, N4, 445–453.
Kuznetsov, Y. G. & Malkin, A. J. (1997). Private communication.
Kuznetsov, Y. G., Malkin, A. J., Greenwood, A. & McPherson, A. (1995). *J. Struct. Biol.* **114**, 184–196
Land, T. A., DeYoreo, J. J. & Lee, J. D. (1997). *Surf. Sci.* **84**, 136–155.
Land, T. A., Malkin, A. J., Kuznetsov, Yu. G., McPherson, A. & DeYoreo, J. J. (1995). *Phys. Rev. Lett.* **75**, 2774–2777.
Lemmlein, G. G. (1973). *Morfologiya i Genezis Kristallov* (*Morphology and Genesis of Crystals*), pp. 26–47, 91–99. Moscow: Nauka. (In Russian.)
Malkin, A. J., Kuznetsov, Y. G., Chernov, A. A. & McPherson, A. (1998). Unpublished.
Malkin, A. J., Kuznetsov, Y. G., Glantz, W. & McPherson, A. (1996). *J. Phys. Chem.* **100**, 11737–11743.
Malkin, A. J. & McPherson, A. (1994). *Acta Cryst.* D**50**, 385–395.
Matsuura, Y., Hata, Y., Yamaguchi, T., Tanaka, N. & Kakado, M. (1979). *J. Biochem.* **85**, 729–737.
Mikheev, L. V. & Chernov, A. A. (1987). *Sov. Phys. JETP*, **65**, 971–977.
Mikheev, L. V. & Chernov, A. A. (1991). *J. Cryst. Growth*, **112**, 591–596.
Nakada, T., Miyashita, S., Sazaki, G., Komatsu, H. & Chernov, A. A. (1996). *Jpn J. Appl. Phys.* **35**, L52–L55.
Oki, H., Matsuura, Y., Komatsu, H. & Chernov, A. A. (1998). *Acta Cryst.* D. In the press.
Ovsienko, D. E. & Alfintsev, G. A. (1980). *Crystals. Growth Properties and Applications*, Vol. 2, pp. 119–169. Berlin: Springer.
Punin, Y. O. (1981). *Zapiski Vses. Mineral. Obsh.* **110**, N6, 666–687. (In Russian.)
Punin, Y. O. (1983). *Kristallov Rost*, edited by E. I. Giavargizov & S. A. Grinberg, Vol. 14. (In Russian.) Engl. transl: *Growth of Crystals*, pp. 108–117. New York: Consultants Bureau.
Punin, Y. O. (1994). *Zh. Strukt. Khim.* **35**, N5, 50–59. (In Russian.)
Punin, Y. O. & Gorskaya, M. G. (1992). *Mineral. J.* **14**, 36–43. (In Russian.)
Punin, Y. O. & Ivanova, T. Y. (1993). *Zh. Strukt. Khim.* **35**, N6, 99–107. (In Russian.)
Rashkovich, L. N. (1991). *KDP Family Single Crystals.* Bristol: Adam Hilger.
Rashkovich, L. N., Grozdev, N. V. & Yaminshi, I. V. (1998). *Crystallogr. Rep.* In the press.
Reid, R. C., Prausnitz, J. M. & Sherwood, T. K. (1985). *The Properties of Gases and Liquids.* New York: McGraw-Hill.
Robinson, I. K. (1986). *Phys. Rev. B*, **33**, 3830–3836.
Rosenberger, F., Vekilov, P. G., Mushol, M. & Thomas, B. R. (1996). *J. Cryst. Growth*, **168**, 1–27.
Shtukenberg, A. G., Punin, Y. O. & Kotelnikova, E. N. (1993). *Zapiski Vsesoyuznogo Meineralogicheskovb Obshchesta*, N5, 53–63. (In Russian.)
Simonov, V. I. (1992). *Structural Crystallography*, pp. 21–42. Moscow: Nauka. (In Russian.)
Smol'skii, I. L., Chernov, A. A., Kuznetsov, Y. G., Parvov, V. F. & Rozhanskii, V. N. (1984). *Sov. Phys. Dokl.* **29**, 703–706.
Smol'sky, I. L., Voloshin, A. E. & Rudneva, E. B. (1996). *Acta Cryst.* A**52**, C508.
Vekilov, P. G., Alexander, J. L. & Rosenberger, F. (1996). *Phys. Rev. E*, **54**, 6650–6660.
Vekilov, P. G., Ataka, M. & Katsura, T. (1993). *J. Cryst. Growth*, **130**, 317–320.
Vekilov, P. G., Kuznetsov, Yu. G. & Chernov, A. A. (1992). *J. Cryst. Growth*, **121**, 643–655.
Vekilov, P. G., Lin, H. & Rosenberger, F. (1997). *Phys. Rev. E*, **55**, 3202–3214.

Vekilov, P. G. & Rosenberger, F. (1998). *Phys. Rev. E*, **57**, 67–79.
Volmer, M. (1939). *Kinetik der Phasenbildung.* Berlin: Steikopf Verlag.
Voloshin, A. E., Smol'sky, I. L. & Sorokin, S. S. (1996). *Acta Cryst.* A**52**, C369.
Voloshin, A. E., Smol'sky, I. L., Sorokin, S. S. & Rudneva, E. B. (1998). *J. Cryst. Growth.* In the press.
Voronkov, V. V. (1973). *Sov. Phys. Crystallogr.* **18**, 21–23.
Watring, D. A. & Lehoczky, S. L. (1996). *J. Cryst. Growth*, **167**, 478–487.
Zaitseva, N. P., DeYoreo, J. J., Dehaven, M. R., Vital, R. L., Montgomery, K. E., Richardson, M. & Atherton, M. J. (1997). *J. Cryst. Growth*, **180**, 255–262.
Zhurova, E. A., Maximov, B. A., Simonov, V. I. & Sobolev, B. P. (1996). *Crystallogr. Rep.* **41**, 413–418.